ADVANCED MATERIALS

[1] S. Diele, P. Göring, in *Handbook of Liquid Crystals* (Eds: D. Demus, J. Goodby, G. W. Gray, H.-W. Spiess, V. Vill), Vol. 2B, Wiley-VCH, Weinheim **1998**, p. 887.
[2] F. Reinitzer, *Monatsh. Chem.* **1888**, *9*, 421.
[3] P. P. Crooker, in *Chirality in Liquid Crystals* (Ed: H. S. Kitzerow, C. Bahr), Springer, Heidelberg **2001**, Ch. 7.
[4] a) M. H. Li, H. T. Nguyen, G. Sigaud, *Liq. Cryst.* **1996**, *20*, 361. b) M. H. Li, V. Laux, H. T. Nguyen, G. Sigaud, P. Barois, N. Isaert, *Liq. Cryst.* **1997**, *23*, 389.
[5] B. A. DiDonna, R. D. Kamien, *Phys. Rev. Lett.* **2002**, *89*, 215 504.
[6] L. G. Fel, *Phys. Rev. E* **1995**, *52*, 702.
[7] L. Radzihovsky, T. C. Lubensky, *Europhys. Lett.* **2001**, *54*, 206.
[8] D. Vorländer, *Z. Phys. Chem. (Leipzig)* **1923**, *105*, 211.
[9] a) Y. Matsunaga, S. Miyamoto, *Mol. Cryst. Liq. Cryst.* **1993**, *237*, 311. b) H. Matsuzaki, Y. Matsunaga, *Liq. Cryst.* **1993**, *14*, 105.
[10] T. Niori, T. Sekine, J. Watanabe, T. Furukawa, H. Takezoe, *J. Mater. Chem.* **1996**, *6*, 1231.
[11] D. R. Link, G. Natale, R. Shao, J. E. Maclennan, N. A. Clark, E. Körblova, D. M. Walba, *Science* **1997**, *278*, 1924.
[12] G. Pelzl, S. Diele, W. Weissflog, *Adv. Mater.* **1999**, *11*, 707.
[13] A. Jákli, D. Krüerke, H. Sawade, G. Heppke, *Phys. Rev. Lett.* **2001**, *86*, 5715.
[14] D. M. Walba, E. Korblova, R. Shao, J. A. Meclennan, D. R. Link, M. A. Glaser, N. A. Clark, *J. Phys. Org. Chem.* **2000**, *13*, 830.
[15] G. Pelzl, A. Eremin, S. Diele, H. Kresse, W. Weissflog, *J. Mater. Chem.* **2002**, *12*, 2591.
[16] M. Y. M. Huang, A. M. Pedreira, O. G. Martins, A. M. Figueiredo Neto, A. Jákli, *Phys. Rev. E* **2002**, *66*, 031 708.
[17] K. Fodor-Csorba, A. Vajda, G. Galli, A. Jákli, D. Demus, *Macromol. Chem. Phys.* **2002**, *203*, 1556.
[18] K. D'Have, A. Dahlgren, P. Rudquist, J. P. F. Lagerwall, G. Andersson, M. Matuszczyk, S. T. Lagerwall, R. Dabrowski, W. Drzewinski, *Ferroelectrics* **2000**, *244*, 115.
[19] A. Jákli, G. G. Nair, S. Abeygunaratne, R. P. Sun, C. K. Lee, L. C. Chien, *Ferroelectrics* **2002**, *276*, 135.
[20] A. Jákli, L.-C. Chien, D. Krüerke, H. Sawade, G. Heppke, *Liq. Cryst.* **2002**, *29*, 377.
[21] G. Heppke, A. Jákli, S. Rauch, H. Sawade, *Phys. Rev. E* **1999**, *60*, 5575.
[22] A. Jákli, S. Rauch, D. Lötzsch, G. Heppke *Phys. Rev. E* **1998**, *57*, 6737.
[23] a) S. V. Shilov, S. Rauch, H. Skupin, G. Heppke, F. Kremer, *Liq. Cryst.* **1999**, *26*, 1409. b) M. Zennoyoji, Y. Takanashi, K. Ishikawa, J. Thisayukta, J. Watanabe, H. Takezoe, *Mol. Cryst. Liq. Cryst.* **2001**, *366*, 693.
[24] T. Sekine, Y. Takanashi, T. Niori, J. Watanabe, H. Takezoe, *Jpn. J. Appl. Phys.* **1997**, *36*, 6455.
[25] J. Thisayukta, Y. Nakayama, S. Kowauchi, H. Takezoe, J. Watanabe, *J. Am. Chem. Soc.* **2000,** *122*, 7441.
[26] G. Dantlgraber, A. Eremin, S. Diele, A. Hauser, H. Kresse, G. Pelzl, C. Tschierske, *Angew. Chem.* **2002**, *41*, 2408.

Nanoporous Structures Prepared by an Electrochemical Deposition Process**

By *Heon-Cheol Shin*, *Jian Dong*, and *Meilin Liu**

Ramification of electrodeposited metals such as copper and tin has been a very intriguing topic for several decades from both the scientific and the technological point of view.[1,2] In particular, three-dimensional (3D) nanoramified metal deposits are ideally suited for electrodes in electrochemical devices such as fuel cells, batteries, and sensors. The open porous structure allows rapid transport of gas and liquid, while the extremely high surface area is desirable for electrochemical reactions. To date, however, most studies have focused just on avoiding the ramification of these metal deposits, as needed for the intended applications in electronic devices.[2–4] The potential applications of these unique structures in electrochemical devices are yet to be explored.

While an electrodeposition process can easily create a 3D dendritic structure of metals, it is very difficult to control the microstructure with desired features. The trunks and branches in the porous dendritic structure are often unable to support the weight of numerous sub-branches, leading to collapses on itself in the electrolyte solution even with minimal convective forces. Furthermore, dendritic structures are easily overgrown to become a thick film with very low porosity, making it difficult for gas/liquid to transport through as required in electrochemical applications.

In this communication, we report a unique method to overcome the above problems in order to make self-supported nanoramified (dendritic) deposits. This simple but very effective technique involves electrochemical deposition accompanying hydrogen evolution, which has been deliberately suppressed in typical electrodeposition processes to produce dense metallic components. In this process, hydrogen bubbles play a crucial role in the formation of the porous structure; they function as a dynamic negative template. The resulting structures are 3D free-standing foams of metals (such as copper and tin) with highly porous ramified (dendritic) walls. A recent study by Zach and Penner[5] has been also based upon a hydrogen co-evolution process. However, they have obtained just two-dimensional (2D) nanocrystalline nickel and the role of hydrogen evolution on electrochemical deposition (i.e., the size-selective deposition of nanoparticles) is quite different from the role of hydrogen evolution in this work.

Shown in Figure 1 are some typical SEM (Hitachi S-800 FEG Scanning Electron Microscope) images of porous copper deposits created by electrodeposition for different periods of time. Clearly, the pore size of the 3D microfoam structure increased with the time of deposition (or the distance from the substrate). More importantly, the walls of the microfoam are also highly porous due to vigorous hydrogen evolution originated not only at the substrate but also at the deposited copper dendrites.

Schematically shown in Figure 2 is a simplified description of the formation process of the metal foams. The hydrogen bubbles, originating from the cathodic reaction on copper substrate, create a continuous path from the substrate to the electrolyte–air interface during the deposition process. Where there is a bubble, there will be no deposition of metals simply because there are no metal ions available. Thus, the numerous hydrogen bubbles evolved at different locations on the substrate generate the pores in the deposits. When the deposition rate is sufficiently high, the concentration of metal ions in the vicinity of the metal deposits is quickly depleted, and concomitantly incessant gas evolution disrupts the diffusion of

[*] Prof. M. Liu, Dr. H.-C. Shin, Dr. J. Dong
Center for Innovative Fuel Cell and Battery Technologies
School of Materials Science and Engineering
Georgia Institute of Technology
Atlanta, GA 30332-0245 (USA)
E-mail: meilin.liu@mse.gatech.edu

[**] This work was supported by Office of Science, Department of Energy under Grant No. DE-FG02-01ER15220.

  DOI: 10.1002/adma.200305160

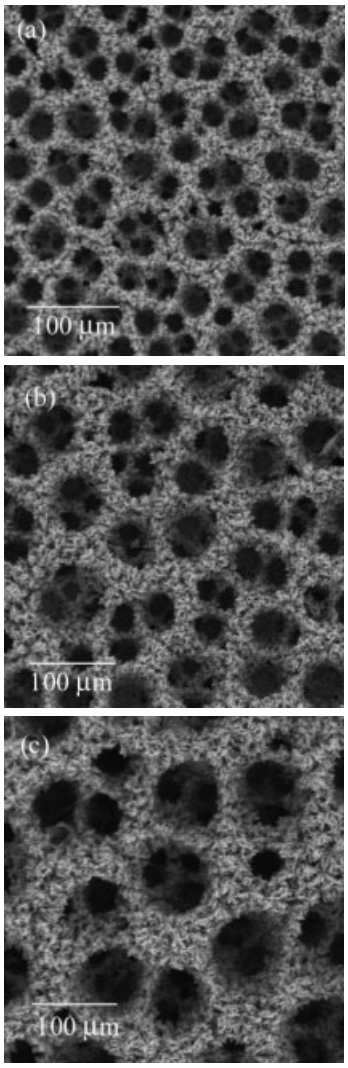

Fig. 1. Typical SEM images of porous copper deposits created by electrodeposition for different periods of time: a) 5 s, b) 10 s, c) 20 s. The surface pore size of the 3D foam structure increased with the time of deposition (or the distance from the substrate).

reactive ions from bulk electrolyte to ion-depleted region. As moving bubbles open up a path, the growth of metal takes its way between gas bubbles. Consequently, a series of gas bubbles acts as a dynamic negative template during the course of metal growth, leaving metal deposits between gas bubbles (foam structure). Here, the pore size of the foam increases with the distance away from the substrate because of the coalescence of hydrogen bubbles (see Fig. 2), creating structures ideally suited for electrodes in fuel cells, batteries, and sensors.

Depending on the choice of the substrate and the porous metallic electrodes to be deposited, the actual deposition process could be more complicated. In the case of copper deposition, for example, hydrogen bubbles evolved from the substrate create the large pores while the hydrogen bubbles liberated from the freshly formed porous deposits create nanopores as deposits form. In contrast, in the case of tin deposition, hydrogen bubbles are generated mostly from the copper substrate due to a higher hydrogen overvoltage on tin.[6]

Figure 3 depicts the 3D foam structures of copper and tin deposits at different magnifications. The overall macroscopic features of the copper deposits are similar to those of the tin deposits. The foam walls are composed of numerous small-ramified coppers (Fig. 3a) or dendritic tins (Fig. 3b). It is noted that overgrowing (too dense) or preferential growing (e.g., perpendicular to the substrate) was not observed. The feature size of the branches in copper and tin deposits are of the order of hundreds of nanometers (Figs. 3e,f). It is also found that the porous deposits are crosslinked (networked) ramified (dendritic) products in all directions throughout the walls (Figs. 3c,d), leading to a mechanically well-supported structure. In fact, the porous deposits of both copper and tin always maintained the structural integrity during handling in the electrolyte and subsequent procedures for drying and characterization.

As we further examine the detailed microscopic features of the copper and tin deposits, two subtle differences are observed. One difference in morphology between copper and tin deposits is the shape of the branches. The branches of the tin deposits are longer and straighter than those of the copper deposits, as can be seen from Figures 3e,f. This result is consistent with previous reports, where the typical copper and tin dendritic structures have been explained on the basis of diffusion-limited aggregation (DLA)[7] and surface relief phenomenon,[8] respectively.

Another difference in detailed microstructure of the two deposits is that the branches of the copper foams contain nanosized grains (and pores) whereas the branches of the tin deposits are relatively dense. Shown in Figure 4a is the TEM (Hitachi HF-2000 transmission electron microscope) image of the branch, revealing that the copper branches consist of copper particles of several tens of nanometers. It is conceivable that hydrogen bubbles are liberated from the copper deposits as they form, creating nanoparticles of copper (or nanopores in the copper deposits). In contrast, no small grains (and pores)

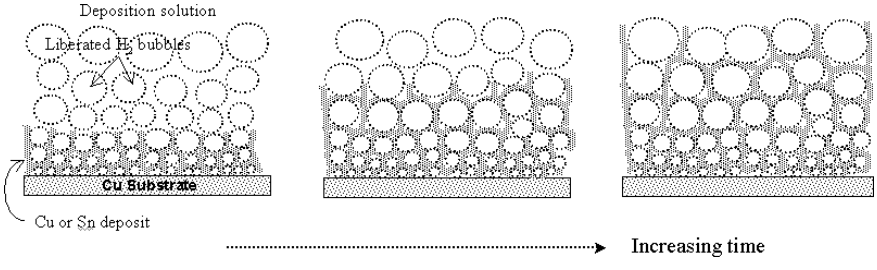

Fig. 2. Simplified description of the formation process of the metal foams. A series of gas bubbles, evolved at different locations on the substrate, acts as a dynamic negative template during the course of metal growth, leaving metal deposits between gas bubbles (foam structure). Here, the pore size of the foam increases with the distance away from the substrate because of the coalescence of hydrogen bubbles.

ADVANCED MATERIALS

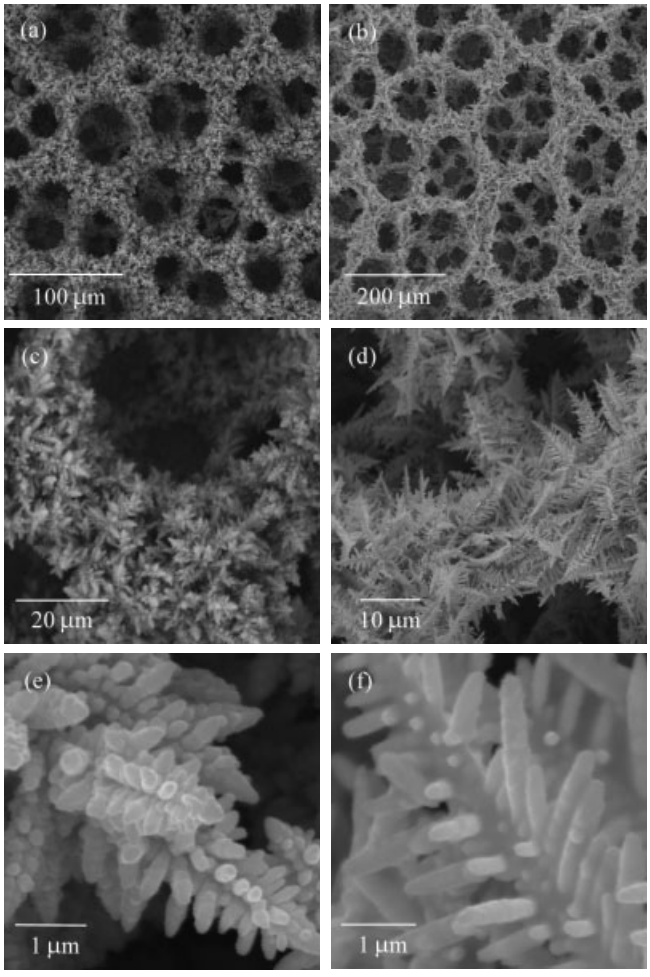

Fig. 3. 3D foam structures of copper (a,c,e), and tin (b,d,f) deposits at different magnifications. The copper and tin foam structures have been prepared by an electrodeposition for 20 s and 5 s, respectively.

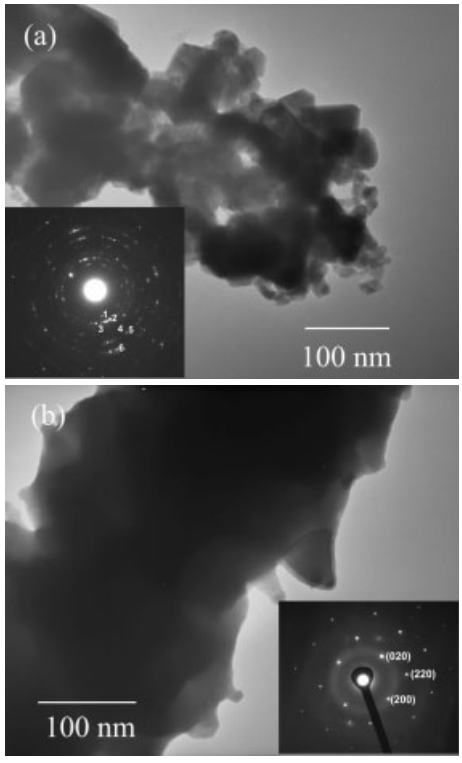

Fig. 4. TEM images of a) copper and b) tin branches with the corresponding electron diffraction patterns (insets). The numbers on the diffraction pattern in (a) represent 1-Cu_2O (110); 2-Cu_2O (111); 3-Cu (111); 4-Cu (200); 5-Cu_2O (220); 6-Cu (220).

are observed in the dendritic tin branch because no hydrogen was generated on tin deposit due to the high hydrogen overvoltage on tin, as shown in Figure 4b.

The corresponding electron diffraction pattern of the copper deposits, inset in Figure 4a, shows discontinuous rings, indicating the different orientations of the individual particles. Although the diffraction pattern of Cu_2O is also identified along with that of copper, a dark field image with the selected dots of Cu_2O in diffraction pattern shows that Cu_2O diffraction is only due to the oxide on copper surface, which is quite different from a recent report on electrodeposited copper filament,[9] where copper nanocrystallites are separated by copper oxides. Considering the studies on reaction mechanism of electrodeposited copper,[10,11] the absence of copper oxides inside the branches in this work can be attributed to the sufficiently high acidity of the deposition solution. That is, because of the abundant protons in the electrolyte, the growing copper tips always experience the highly acidic atmosphere around them, which suppresses the oxide formation and enhances the reduction of copper to metallic copper.

On the other hand, the polycrystalline copper branch is a characteristic feature of DLA-like copper deposits and its formation mechanism has been proposed on the basis of the oscillatory character in the nucleation kinetics.[12] Additionally, owing to the rigorous gas evolution on growing copper tips in this work, a local turbulence of electrolyte might be created around the copper tips, disrupting continuous growth of the copper tips and promoting the formation of new nuclei with random orientation on the tips. This could be partly responsible for the polycrystalline character of the copper branches. In contrast, TEM image of a tin branch (Fig. 4b) and the corresponding electron diffraction pattern (inset in Fig. 4b) suggest that the tin branch is a single crystal, which is consistent with a previous report on tin whisker.[8]

Shown in Figure 5 are the X-ray diffraction patterns (Philips PW-1800 X-ray diffractometer) of copper and tin deposits (scratched off from the substrates), indicating that the copper deposits have a face-centered cubic (fcc) structure while the tin deposits have a tetragonal structure with high crystallinity.

Shown in Figure 6 are the thicknesses of the deposits, average diameters of the pores on the surface, and the amounts of deposits (in mmol cm^{-2}) as a function of deposition time. The deposition rates (in thickness per unit time) of the copper (open circle) and the surface pore size (open square) are much smaller than those of the tin deposit (solid circle and square) under similar conditions. For example, to achieve sim-

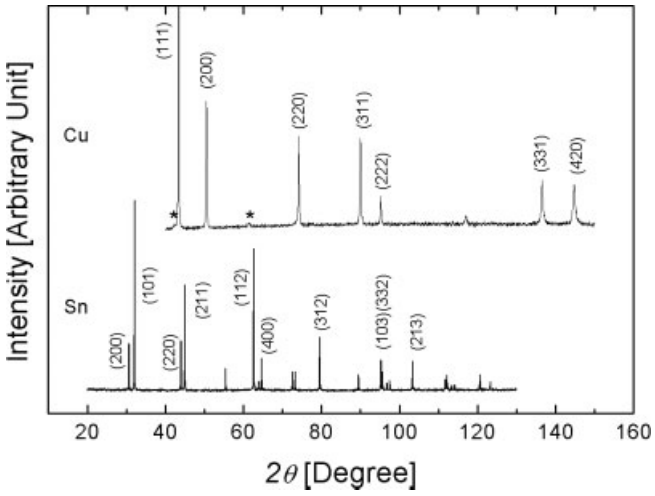

Fig. 5. X-ray diffractograms of copper (upper) and tin (lower) powders scratched from the substrates showing high crystallinities of the deposits. Only main peaks have been indexed. Small Cu_2O peaks (*) have been also identified from the XRD pattern of copper (For details, see Fig. 4 and the corresponding explanation in the text). The quantitative analysis of a full width at half maximum (FWHM) data showed that the primary particle size of tin is at least five times larger than that of copper, which is indeed consistent with the TEM results in Figure 4. Further details of the crystal structure investigation(s) may be obtained from the Fachinformationszentrum Karlsruhe, D-76344 Eggenstein-Leopoldshafen, Germany, on quoting the depository numbers CSD-413067 (Cu) and 413068 (Sn).

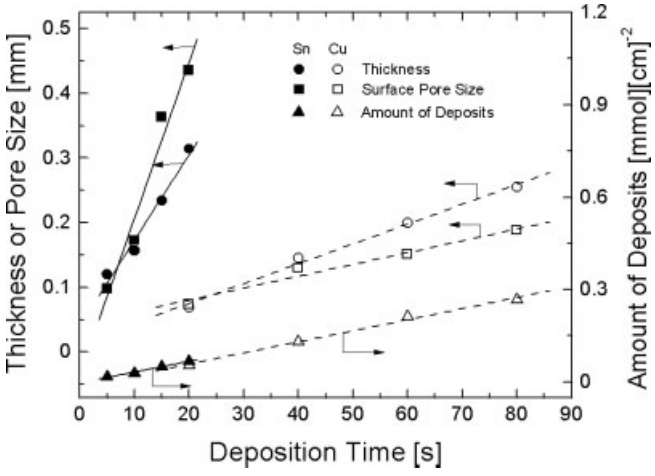

Fig. 6. Dependence of thicknesses of the deposits (circles), average diameters of the surface pore (squares), and amount of the deposits (triangles) on deposition time. The current efficiency of the electrochemical deposition process is about 35 % for both copper and tin deposition.

ilar thickness, the time needed for deposition of copper is about 4 times of that for deposition of tin. However, the apparent density of the deposited porous copper (open triangle) is much higher than that of the porous tin (solid triangle). Analysis of a Cu-deposit prepared by deposition for 40 s indicated that the apparent density (mass/[substrate area × thickness]) of copper is about 0.6 g cm^{-3}; on the other hand, the analysis of a tin deposit prepared by deposition for 10 s indicated that the apparent density is about 0.2 g cm^{-3}. It is noted that the ratio of the apparent densities (0.6 g cm^{-3}:0.2 g cm^{-3}) is far greater than the ratio of the intrinsic densities of the two metals (8.92 g cm^{-3}:7.31 g cm^{-3}). The higher density of copper deposits is due to its lower aspect ratio (length/width). Another interesting point is that the diameters of the surface pores are comparable to (for copper) or larger than (for tin) the thicknesses of the deposits. This implies that the pore is not spherical, but ellipsoidal.

Among the deposition parameters studied, the concentration of the metal ions (especially Sn^{2+}) greatly influences the morphologies of the foam deposits, whereas the acidity and the applied current density had little effect on the foam structure if they are sufficiently high (i.e., > 1.0 M H_2SO_4 and > 0.5 A cm^{-2}). The higher content of tin(II) ions than the optimum amount (0.15 M) resulted in thicker and denser foam walls. Eventually, the pores disappeared completely when the content of tin ions was greater than ~ 0.5 M. On the other hand, if the tin ion content is too low (less than ~ 0.10 M), the walls of tin foam become too thin to form a 3D foam structure. In contrast, the well-defined foam structure with walls of small ramified copper can be created in a relatively wide concentration range of copper ions (from 0.1 to 0.4 M Cu ions).

Nanoporous metallic electrodes have been successfully prepared using an electrodeposition process. This represents a novel way of creating porous structures that allow not only fast transport of gas and liquid but also rapid electrochemical reactions due to high surface area. The porous structures are ideally suited for electrodes in electrochemical devices such as fuel cells, batteries, and chemical sensors. In particular, the porous tin deposits are being directly used as 3D nanoporous anode for lithium batteries and the nanoporous copper deposits are being used for construction of nanocomposite anodes (consisting of Cu and CeO_2) for solid oxide fuel cells. Further, the nanoporous copper deposits can be used as 3D templates for preparation of porous structures of other functional materials, including electrodes for solid oxide fuel cells and solid-state gas sensors.

Experimental

High-purity copper (Alfa Aesar, 99.8 %), cleaned with acetone and dilute hydrochloric acid, was used as the substrate (cathode) for copper and tin deposition. Copper and tin (Alfa Aesar, 98.8 %) plates with a superficial surface area of 5 cm^2 are used as the counter electrodes (anodes) for copper and tin deposition, respectively. The distance between anode and cathode is 2 cm. A constant current (as high as 3 A cm^{-2}) was applied to the substrate using a Solartron 1285 potentiostat in an electrolyte of 1.5 M sulfuric acid (Aldrich) containing 0.20 M copper sulfate (Alfa Aesar) or 0.15 M tin sulfate (Alfa Aesar) at room temperature. Deposition was performed in a stationary electrolyte solution without stirring or N_2 bubbling.

Received: March 25, 2003
Final version: June 16, 2003

[1] E. Ben-Jacob, P. Garik, *Nature* **1990**, *343*, 523.
[2] R. Schetty, *Circuit World* **2001**, *27*, 17.
[3] I. Petersson, E. Ahlberg, *J. Electroanal. Chem.* **2000**, *485*, 166.
[4] B. Kim, T. Ritzdorf, *J. Electrochem. Soc.* **2003**, *150*, C53.
[5] M. P. Zach, R. M. Penner, *Adv. Mater.* **2000**, *12*, 878.
[6] M. Pourbaix, in *Atlas of Electrochemical Equilibrium in Aqueous Solution*, Pergamon Press, Oxford, New York **1966**, p. 475.
[7] T. A. Witten, L. M. Sander, *Phys. Rev. Lett.* **1981**, *47*, 1400.

ADVANCED MATERIALS

[8] George T. T. Sheng, C. F. Hu, W. J. Choi, K. N. Tu, Y. Y. Bong, L. Nguyen, *J. Appl. Phys.* **2002**, *92*, 64.
[9] M. Wang, S. Zhong, X.-B. Yin, J.-M. Zhu, R.-W. Peng, Y. Wang, K.-Q. Zhang, N.-B. Ming, *Phys. Rev. Lett.* **2001**, *86*, 3827.
[10] F. Texier, L. Servant, J. L. Bruneel, F. Argoul, *J. Electroanal. Chem.* **1998**, *446*, 189.
[11] M.-Q. Lopez-Salvans, F. Sagues, J. Claret, J. Bassas, *Phys. Rev. E* **1997**, *56*, 6869.
[12] V. Fleury, *Nature* **1997**, *390*, 145.

Tailoring Discotic Mesophases: Columnar Order Enforced with Hydrogen Bonds**

By *Raluca I. Gearba*, *Matthias Lehmann*, *Jérémy Levin*, *Dimitri A. Ivanov*,* *Michel H. J. Koch*, *Joaquín Barberá*, *Michael G. Debije*, *Jorge Piris*, and *Yves H. Geerts*

Considerable scientific and technological effort has been recently devoted to discotic liquid crystals as functional materials for application as light-emitting diodes,[1] photovoltaic cells,[2] and field-effect transistors.[3] Such interest can be explained by the increased charge carrier mobility in discotics as compared to conventional conjugated polymers.[4] For example, record values of the charge carrier mobility up to 0.5 $cm^2 V^{-1} s^{-1}$ have been obtained for self-organizing hexabenzocoronene mesogens.[5] Generally, the high charge carrier mobility results from the facility of discotics to self-organize into columns thereby maximizing the overlap of frontier orbitals. Recently, a theoretical model was proposed in which the coplanar distance and orientation of two aromatic cores are correlated with their frontier orbital splitting, the latter governing the charge carrier mobility.[6] To improve further the charge-transport properties along the columns, the intermolecular distance should be made as small as possible.[7] The inter-core distances for typical semiconducting columnar mesogens range from 3.5 to 4.0 Å,[8] which roughly corresponds to the sum of the van der Waals radii of carbon atoms.[9] Smaller inter-core distances have been reported for a tricycloquinazoline core (3.29 Å)[10] and for lutetium phthalocyanine dimers (3.26 Å).[11] The latter system having the smallest intracolumnar distance also reveals the highest charge mobility in a hexagonal columnar phase, Col_h, which is attributed to the additional attractive interaction mediated by the Lutetium ion.

Hydrogen bonds have been used as a tool to enhance the attractive interactions between discotic mesogens[12,13] or bisurea compounds.[14] More specifically, it was observed that amide hydrogen bonds serve as non-covalent "clamps" in the crystal phase of hexacarboxamidohexaazatriphenylene (**1a**) (Fig. 1a) and that the resulting π–π distance is as small as 3.32 Å.[15] Disk-shaped molecules (**1b**,**c**) with six hexyl or decyl chains were synthesized as potential mesogens by Czarnik et al., but no thermotropic behavior or structural data were reported (these molecules decompose before the transition to the isotropic phase).[16] Our combined interest in electron deficient mesogens[17] and in discotics with high charge carrier mobility[4] led us to reinvestigate this type of molecule. We report here on discotic mesogen HAT-CONHR, **1d**, for which the formation of hydrogen bonds results in the smallest inter-disk distance (3.18 Å) ever found in columnar liquid crystals, to the best of our knowledge.

The target compound **1d** was obtained by six-fold reaction of dodecylamine with the hexamethylester derivative.[16] The crude product was purified by precipitation from trifluoroacetic acid by cautious addition of water. The structure and purity of the isolated molecule were established by ^1H and ^{13}C NMR spectroscopy, FTIR spectroscopy, mass spectrometry and elemental analysis (see Experimental sec.). Derivative **1d** is found to be poorly soluble in common organic solvents even at high temperatures. Generally, perfect columns exhibiting only their hydrophobic shell to the external environment are expected to be soluble in common non-polar solvents. Therefore, the low solubility of **1d** can be accounted for by structural defects in columnar ordering that might crosslink neighboring columns via hydrogen bonding.[18] Characteristically, ^1H and ^{13}C NMR spectra could only be obtained after addition of a small amount of trifluoroacetic acid to deuterated chloroform, thereby corroborating the hypothesis that formation of hydrogen bonds causes the insolubility.

The mesomorphic behavior of **1d** was studied using differential scanning calorimetry (DSC), polarized optical microscopy (POM) and X-ray diffraction. POM observations reveal birefringence in the whole temperature range under investigation, i.e., from room temperature (RT) up to the degradation temperature (approximately 250 °C). However, no specific texture was observed, which could be due to the fact that the

[*] Prof. D. A. Ivanov, R. I. Gearba
Laboratoire de physique des polymères, CP 223
Universite Libre de Bruxelles
B-1050 Brussels (Belgium)
E-mail: divanov@ulb.ac.be
Dr. M. Lehmann, J. Levin, Dr. Y. H. Geerts
Laboratoire de chimie des polymères, CP 206/1
Université Libre de Bruxelles
Boulevard du Triomphe, B-1050 Brussels (Belgium)
Dr. M. H. J. Koch
European Molecular Biology Laboratory
Hamburg Outstation, EMBL c/o DESY
Notkestrasse 85, D-22603 Hamburg (Germany)
Dr. J. Barberá
Química Orgánica
Facultad de Ciencias-I.C.M. A.
Universidad de Zaragoza-C.S.I.C.
E-50009 Zaragoza (Spain)
Dr. M. G. Debije, J. Piris
Interfaculty Reactor Institute
Delft University of Technology
Mekelweg 15, NL-2629 JB Delft (The Netherlands)

[**] This work was financially supported by the Communauté Française de Belgique (ARC No. 00/05-257), Fonds Emile Defay and through the DISCEL project (G5RD-CT-2000-00321). The synchrotron radiation work was supported by the European Union through the HCMP Access to Large Installation Project, Contract HPRI-CT-1999-00017 to the EMBL-Hamburg. We are grateful to H. Meier and A. Oehlhof for carrying out the MALDI-TOF measurements and the elemental analysis at the University of Mainz and to J. M. Warman, M. P. de Haas, D. Caprion, J. Cornil, M. Baus, and J.-P. Ryckaert for fruitful discussions.

  DOI: 10.1002/adma.200305137